

# Fizeau interferometric cophasing of segmented mirrors: experimental validation

Anthony Cheetham,<sup>1</sup> Nick Cvetojevic<sup>1,2,3</sup> Barnaby Norris,<sup>1</sup> Anand Sivaramakrishnan,<sup>4</sup> and Peter Tuthill<sup>1</sup>

<sup>1</sup>*Sydney Institute for Astronomy, School of Physics, University of Sydney, NSW 2006, Australia*

<sup>2</sup>*Centre for Ultrahigh bandwidth Devices for Optical Systems (CUDOS), Institute of Photonics and Optical Science (IPOS), School of Physics, University of Sydney, Sydney, NSW 2006, Australia*

<sup>3</sup>*Australian Astronomical Observatory, NSW 2121, Australia*

<sup>4</sup>*Space Telescope Science Institute, 3700 San Martin Drive, Baltimore MD 21218, USA*

\* [a.cheetham@physics.usyd.edu.au](mailto:a.cheetham@physics.usyd.edu.au)

**Abstract:** We present an optical testbed demonstration of the Fizeau Interferometric Cophasing of Segmented Mirrors (FICSM) algorithm. FICSM allows a segmented mirror to be phased with a science imaging detector and three filters (selected among the normal science complement). It requires no specialised, dedicated wavefront sensing hardware. Applying random piston and tip/tilt aberrations of more than 5 wavelengths to a small segmented mirror array produced an initial unphased point spread function with an estimated Strehl ratio of 9% that served as the starting point for our phasing algorithm. After using the FICSM algorithm to cophase the pupil, we estimated a Strehl ratio of 94% based on a comparison between our data and simulated encircled energy metrics. Our final image quality is limited by the accuracy of our segment actuation, which yields a root mean square (RMS) wavefront error of 25 nm. This is the first hardware demonstration of coarse and fine phasing an 18-segment pupil with the James Webb Space Telescope (JWST) geometry using a single algorithm. FICSM can be implemented on JWST using any of its scientific imaging cameras making it useful as a fall-back in the event that accepted phasing strategies encounter problems. We present an operational sequence that would co-phase such an 18-segment primary in 3 sequential iterations of the FICSM algorithm. Similar sequences can be readily devised for any segmented mirror.

© 2014 Optical Society of America

**OCIS codes:** (120.3180) Interferometry; (120.6085) Space instrumentation; (110.1080) Active or adaptive optics.

---

## References and links

1. J. E. Nelson, "The University of California 10-m telescope project," *J. Opt. Soc. Am.* , **69**, 1436 (1979).
2. J. E. Nelson, "Design concepts for the California extremely large telescope (CELT)," *Proc. SPIE* , **4004**, 282–289 (2000).
3. R. Gilmozzi, "Science and technology drivers for future giant telescopes", *Proc. SPIE* , **5489**, 1–10 (2000).
4. G. Chanan, M. Troy, F. Dekens, S. Michaels, J. Nelson, T. Mast, and D. Kirkman, "Phasing the mirror segments of the Keck telescopes: the broadband phasing algorithm," *Appl. Opt.* **37**, 140–155 (1998).
5. G. Chanan, C. Ohara, and M. Troy, "Phasing the mirror segments of the Keck telescopes II: the narrow-band phasing algorithm," *Appl. Opt.* **39**, 4706–4714 (2000).

6. D. S. Acton, T. Towell, J. Schwenker, J. Swensen, D. Shields, E. Sabatke, L. Klingemann, A. R. Contos, B. Bauer, and K. Hansen, "Demonstration of the James Webb Space Telescope commissioning on the JWST testbed telescope", *Proc. SPIE* , **6265**, 62650R (2006).
7. D. S. Acton, T. Towell, J. Schwenker, D. Shields, E. Sabatke, A. R. Contos, K. Hansen, S. Fang, D. Bruce and S. Smith, "End-to-end commissioning demonstration of the James Webb Space Telescope", *Proc. SPIE* , **6687**, 6687E (2007).
8. J. R. Fienup, J. C. Marron, T. J. Schulz and J. H. Seldin, "Hubble Space Telescope characterized by using phase-retrieval algorithms", *Appl. Opt.* , **32**, 1747–1767 (1993).
9. A. Sivaramakrishnan, R. Soummer, L. Pueyo, J. K. Wallace and M. Shao, "Sensing phase aberrations behind Lyot coronagraphs", *Astrophys. J.* , **688**, 701–708 (2008).
10. J. E. Krist and C. J. Burrows "Phase-retrieval analysis of pre-and post-repair Hubble Space Telescope images", *Appl. Opt.* , **34**, 4951–4964 (1995).
11. A. Cheetham, *Cophasing JWST's segmented mirror using sparse aperture interferometry* (University of Sydney Hons. Thesis, 2011).
12. A. Cheetham, P. Tuthill, A. Sivaramakrishnan and J. Lloyd, "Fizeau interferometric cophasing of segmented mirrors," *Opt. Express* **20**, 29457–29471 (2012).
13. A. Wirth, "Dispersed Hartmann sensor and method for mirror segment alignment and phasing", <https://www.google.com/patents/US6649895>, US Patent 6,649,895 (2003).
14. F. Shi, C. M. Ohara, G. Chanan, M. Troy and D. C. Redding, "Experimental verification of dispersed fringe sensing as a segment-phasing technique using the Keck Telescope", *Proc. SPIE* , **5489**, 1061–1073 (2004).
15. J. Monnier, P. Tuthill, M. Ireland, R. Cohen, A. Tannirkulam, and M. Perrin, "Mid-infrared size survey of young stellar objects: description of Keck segment-tilting experiment and basic results," *Astrophys. J.* **700**, 491 (2009).
16. E. Sabatke, J. Burge, and D. Sabatke, "Analytic diffraction analysis of a 32-m telescope with hexagonal segments for high-contrast imaging," *Appl. Opt.* **44**, 1360–1365 (2005).
17. M. Helmbrecht, M. He, T. Juneau, M. Hart, and N. Doble, "Segmented MEMS deformable-mirror for wavefront correction", *Proc. SPIE* , **6376**, 63760D (2006).
18. J. Daniel, T. Hull and J. B. Barentine, "JWST: Tinsley achievements on the largest beryllium polishing project", *Proc. SPIE* , **8450**, 845021 (2012).
19. C. Neyman, R. Flicker, S. Pantelev, "Effect of Keck segment figure errors on Keck AO performance", *Keck Adaptive Optics Note* 469 (2007).
20. M. Helmbrecht, M. He, C. Kempf, and M. Besse, "MEMS DM development at Iris AO, Inc.", *Proc. SPIE* , **7931**, 793108 (2011).

## 1. Introduction

Optical and infrared astronomy has long been dominated by a drive for ever larger telescope apertures. Inevitably, this leads to problems with primary mirror rigidity when a single monolithic mirror is used. This has been ameliorated through the use of a segmented primary mirror, first successfully implemented in the optical and near-IR at the Keck Telescopes and now an integral part of modern large telescope design [1–3].

To function as a primary mirror, all segments must be aligned to conform to a single optical surface, a process known as cophasing. Several methods are currently used today. Chanan et al. [4, 5] utilize a modified Shack-Hartmann sensor to measure discontinuous (segmented) wavefronts. Acton et al. [6, 7] use a combination of sensing discontinuities between neighbouring segments and focus-diverse phase retrieval [8]. When implemented, these methods often require dedicated hardware such as actuated elements and additional optics, which introduce non-common path errors. This means that the final science image on the detector has different aberrations than those sensed by the cophasing strategy. Non-common path errors are a concern for many modern astronomical instruments using active or adaptive optics because they create the best wavefront quality at the wavefront sensor rather than the science detector, degrading the performance of scientific instruments [9]. An approach employed on the Hubble Space Telescope utilizes defocus introduced by moving the secondary mirror [10]. Such secondary mirror motions increase risk, especially on space telescopes.

We proposed a new cophasing solution that utilises an interferometric approach to overcome many of these challenges [11, 12]. Our method, Fizeau Interferometric Cophasing of Segmented Mirrors (FICSM), allows a primary mirror to be cophased using any science camera equipped

with three filters; usually those already present for the core science of the instrument. This method has obvious applications in space-based segmented telescopes such as the James Webb Space Telescope (JWST) – where the dedicated hardware required by its proven cophasing techniques introduce some risk of single-point failure. JWST will carry two copies of its wavefront sensing camera (NIRCam) to mitigate this risk.

FICSM could also be applied to cophase ground based segmented telescopes with a few modifications. Short integration times on bright stars are required to freeze seeing-induced fringe motion, and a time-series of such phase measurements averaged to separate wavefront distortion terms due to imperfectly-aligned optics from the random phase scatter due to atmospheric turbulence. Preliminary simulations show that this strategy is successful, although further optimizations for the seeing-limited case are possible but beyond the scope of the present paper.

The accepted coarse phasing method aboard JWST, Dispersed Hartmann Sensing [13], is based on a modified Shack-Hartmann approach with a dispersive element to solve the problem of phase-wrapping. This allows phasing to be accomplished with a science camera. It requires dedicated hardware, and introduces a division of phasing into coarse and fine regimes. FICSM addresses these issues by phasing mirror segments in non-redundant groups. In order to cophase an entire mirror, FICSM either needs to actuate segments or use several pupil masks. A possible alternative to Dispersed Hartmann Sensing for JWST exists [14], although it requires a large number of large segment motions. This alternative approach increases mission risk and operational complexity, given that large actuator motions are often insufficiently accurate. Actuator motions required by FICSM lie within JWST's planned actuator use (both range of motion as well as number of moves), as it is a replacement for the stage when every segment point-spread function (PSF) is co-located at one place on the science detector [6].

Here we report an experimental demonstration of FICSM using an optical testbed. The three-ring segment pattern of the JWST primary mirror was used, along with potential segment groupings that allow the entire mirror to be phased in 3 steps. In an important extension to previous work, we have eliminated the requirement for a pupil-plane mask in favour of full segment interference patterns, using the proven segment-tilting technique [15]. Since FICSM moves segments it is proposed as a commissioning rather than routine phasing method.

Unless otherwise noted, our piston and tip/tilt aberrations are measured at the wavefront rather than on a mirror surface.

## 2. Fizeau interferometric cophasing of segmented mirrors

A detailed explanation of FICSM can be found in the literature [11, 12], although we present a concise summary of the method below.

FICSM involves directly simulating the effects of piston and tip/tilt on a telescope point spread function (PSF) using collimated starlight, in the case where the primary mirror is made up of a non-redundant array of subapertures (for example, whole segments or holes in an aperture mask). The non-redundancy of baseline vectors connecting every pair of subapertures is essential for this method, as it allows the relative pistons and tilts to be measured from each set of interference fringes which are uniquely separable in the image Fourier transform.

The PSF will consist of an envelope function from each subaperture (an Airy pattern in the case of circular holes), and areas where the envelope functions overlap will host interference fringes with a frequency and direction determined by the separation vector between the two subapertures in the telescope pupil.

The presence of a phase step between two subapertures will cause the fringes for that baseline to shift. Large pistons (on the order of a coherence length) will cause polychromatic fringes to blur. This leads to *bandwidth smearing*, a reduction in fringe amplitude and introduces a distribution of phase that is a complicated yet predictable function of piston. The combination

of amplitude and phase distributions produces a unique fingerprint that allows the piston term to be recovered with high accuracy even in the presence of large pistons (up to several filter coherence lengths). By using the distribution of phase and amplitude as a function of spatial frequency in the presence of a polychromatic light source, problems with phase wrapping are avoided.

Introducing a tilt to a subaperture will cause its envelope function to move, both reducing the amplitude of the fringes and introducing a distribution of phase. Our algorithm therefore requires a way to distinguish segment tilts from pistons, as both can produce similar effects.

These effects can be easily separated by measuring tilts using an image taken with a monochromatic source or narrowband filter (simulations show a filter with 1% fractional bandwidth is sufficient). In this case, pistons only contribute as a constant phase offset, with no loss of coherence while tilts produce a simple phase ramp. After tilts have been corrected, a broad bandwidth filter is used to measure the pistons. The amplitude and the shape of the phase distribution allows for a good estimate of the coarse piston, while the average phase allows fine measurement to sub-wavelength precision. To ensure reliability, pistons can be measured using two images taken with different filters. Estimates very occasionally exhibit an ambiguity which can lead to a phasing error of a small integer number (typically 1) of wavelengths, however the use of dual wavelength data completely removes any ambiguity and all such problem cases can be flagged and corrected.

By applying this strategy numerically to a model of JWST NIRCam's long wavelength arm and its complement of filters, it was shown that FICSM has the potential to phase a mirror from an initial state with  $300\ \mu\text{m}$  pistons (corresponding to more than 3 coherence lengths or 70 wavelengths) and tilts as large as 0.5 arcseconds ( $3.5\ \lambda/D$ ) at the wavefront. After 2 applications of FICSM, the wavefront error was reduced by more than 5 orders of magnitude to 3.65 nm RMS, with RMS pistons and tilts of 0.75 nm and 3.7 mas respectively, corresponding to a Strehl ratio of approximately 0.99997 at  $4\ \mu\text{m}$ .

While previous work on FICSM has used circular subapertures (assumed to be in a pupil plane mask), here we employ the hexagonal mirror segments themselves. Since all shapes with straight edges possess analytic Fourier transforms [16], all that is required is to substitute the Airy pattern for its hexagonal equivalent.

### 3. Segment groupings

In order to phase an entire mirror with FICSM, segments must be phased in non-redundant groups. For the case of JWST, these are groups of 3 or 4 segments, as shown in Fig. 1. In principle it is possible to cophase several segment groups at once by tilting them to different positions on the detector, but due to the limited range of motion of our mirror segments, demonstration of this was not possible here. Regardless, the groups used allow the entire mirror to be phased in 3 steps if multiple pointings are possible, or 7 steps if not. The blue group in the first step (segments 1, 3 and 5) are phased with respect to each other first, and then with the remainder of the segments in the third step. These three segments would allow the telescope to guide on a phased PSF in the second step, to improve telescope guiding during its early stages of commissioning. The short baselines between segments 1, 3 and 5 may enable the phasing process to be more robust to telescope jitter, since the fringes formed by this group are correspondingly wide. If multiple pointings are not possible, telescope guiding can be accomplished on a phased PSF after the first step even without this group, and so it can be removed.

Due to the fact that the spatial frequency of interference fringes scales with wavelength, large bandwidths cause a greater range of frequencies to be associated with each baseline - a process known as "bandwidth smearing". This can cause redundancy, as a spatial frequency associated with one baseline at one wavelength can be equal to the spatial frequency associated with

another baseline at a different wavelength. For this grouping of segments, a manageable level of redundancy should be provided at fractional bandwidths up to 25% of the central wavelength. Thus FICSM enables any of JWST's three scientific imaging cameras to cophase JWST, using their standard complement of filters.

The sequence of segment groupings comprising the phasing strategy illustrated in Fig. 1 minimises mirror movement, and mitigates against unexpectedly high jitter when guiding on a broad, single-segment PSF at the start of the commissioning operations. The first group of green segments are initially phased together to define a single "zero" piston position, then all other segments measured relative to this phased group. This avoids the problem of having to move whole groups of phased segments at the end of the phasing sequence. This segment grouping scheme allows an 18 segment mirror to be cophased by moving each segment a maximum of 8 times, with the majority of segments requiring 6 or fewer moves, assuming perfect actuation. In reality larger steps might require iteration similar to JWST's current segment stacking plans [6]

Choosing optimal segment groupings to weave into a phasing sequence requires consideration of a number of factors. Incorporating as many segments as possible in each group allows for a smaller number of steps and groups, but non-redundancy here enforces an upper limit of 4. Starting with an initial group to act as a zero point for subsequent groups decreases the number of actuator moves required, but does not allow for multiple groups to be phased in the first step. The minimum number of such groups also increases with the number of mirror segments.

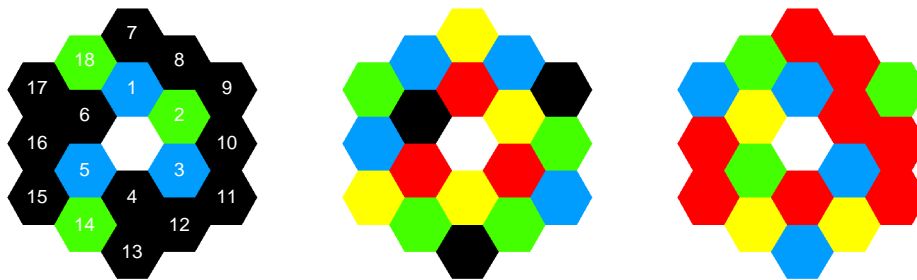


Fig. 1: The segment groups used for this demonstration. Each image shows several segment groups that are phased simultaneously. At each step, each group is shown in a different colour. Red segments are phased but unused in that step and could be used for telescope guiding (to ensure the PSF remains stationary), while black segments are unphased and unused in that step. Each group produces an interference pattern with acceptable levels of redundancy at bandwidths of up to 25% of the peak wavelength. If multiple pointings are possible this allows the entire mirror to be phased in the three steps shown. If this is not possible, the first blue group is unnecessary and the procedure is accomplished in 7 steps. The segment numbering scheme is also shown superimposed on the segments in the first step.

#### 4. Experimental setup

The backbone of our testbed was a 37-element Micro-Electro-Mechanical System (MEMS) segmented mirror from IrisAO. The gold-plated mirrors are arranged in a 4-ring honeycomb configuration and can each be adjusted electronically in piston, tip and tilt to a precision of a few nm [17]. Only the 18 segments in the two middle rings were used, to conform to the layout of the JWST primary mirror. This was accomplished by tilting the remaining segments to a

large beam deviation such that they did not contribute to the PSF. An opaque mask matched to the segment layout was also placed in front of the MEMS chip to block light reflected from other surfaces, minimising the contribution of stray light to the final image.

The MEMS mirror used in this test was expected to have high optical quality, with 6-20nm rms figure error (after removal of piston, tip and tilt aberrations) [17]. This is similar to the measured segment figure error of the JWST primary mirror segments (13.5nm rms) [18], both of which are significantly better than the Keck segments (80 nm rms) [19]. When combined with the operating wavelengths ( $\sim 500$  nm for this setup,  $\sim 4 \mu\text{m}$  for JWST), the phases introduced by segment figure errors in this setup are larger than those expected during JWST phasing and equivalent to phasing the Keck telescopes at  $6 \mu\text{m}$ . Simulations show that segment figure errors may set an upper limit to the accuracy obtainable through FICSM, but including known segment errors into the image simulation code has been shown to effectively ameliorate this problem.

A schematic diagram of the experimental setup is given in Fig. 2. Collimated light was reflected off the MEMS mirror and then focused through a 200 mm focal length achromatic doublet lens (Thorlabs AC254-200-A-ML) onto a Point Grey CCD optical camera. The combination of lens focal length and CCD pixel size ensured the PSF was sampled at more than twice the Nyquist limit, but it is important to note that FICSM operates as long as the sampling is at or above the Nyquist frequency. Our test was performed in the optical band (500-700nm), to increase the amount of wavefront error possible from the limited MEMS absolute range of motion (max.  $5 \mu\text{m}$  in piston).

As described previously, to ensure reliability FICSM requires two broad bandwidth filters and one narrow bandwidth filter. For our demonstration we used a 550 nm (green) and a 650 nm (red) filter, both with a 40 nm bandwidth. A halogen lamp served as a light source for these filters. For our narrow filter we opted for the convenience of a HeNe laser, with a 633 nm central wavelength and negligible bandwidth. This avoided problems with source brightness when combining the halogen lamp with a narrowband filter.

The filters were placed directly between the lamp and a multimode fibre, which was then coupled into a single mode fibre to serve as an analogue of a point source (unresolved star) seen by a telescope. Light from the single mode fibre was collimated using an off-axis parabolic reflective collimator, with the beam then steered onto the MEMS mirror array.

While the 4.0 mm diameter of our Gaussian input beam slightly overfilled the 3.5 mm MEMS mirror array, variations in intensity between segments were significant enough that the intensity profile could not be considered to approximate uniform illumination (as would be expected for a star). To correct for this, the amplitudes of each set of fringes was measured from the narrowband images, as a fraction of their theoretical amplitudes. These multiplicative factors were then applied to each set of fringes for subsequent theoretical images, in essence calibrating the fringes for visibility loss induced by the uneven pupil illumination.

## 5. Procedure and calibration

As with any experimental setup, calibration steps were required to maximise and fully characterise the expected performance of the experiment. Images were dark subtracted and combined from 100 short exposure images to ensure high signal-to-noise out to and beyond the first Airy ring.

Since FICSM cophases segments in groups, at any given step, unwanted segments were “stowed” by tilting them away from the primary PSF into a widely spaced ring. The limited actuation of the MEMS meant that this ring was still within the field of view of the camera. To prevent this source of stray light from biasing the results, frames were taken with the light source on and all segments in their stowed positions. While this subtraction method was not

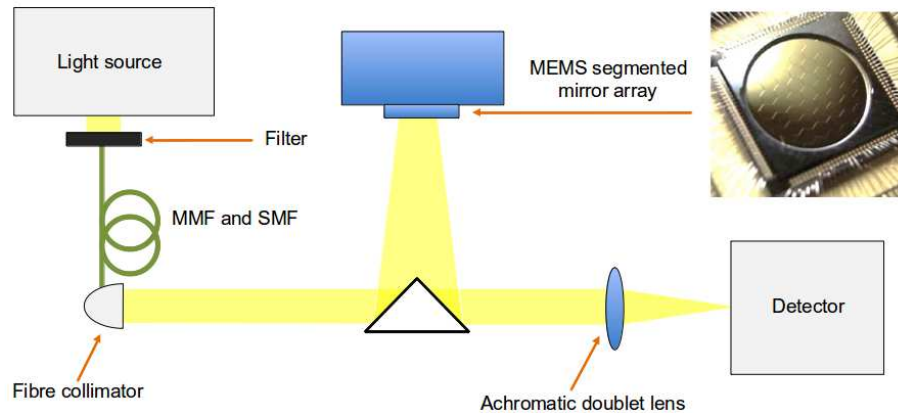


Fig. 2: A schematic overview of the experimental setup. For the broadband images, light from a halogen lamp was passed through a filter into a multimode fibre, then coupled into a single mode fibre connected to a fibre collimator. For the narrow band images, a HeNe laser was connected to the fibre collimator using a single mode fibre only. Collimated light was then reflected off the MEMS mirror array and through an achromatic doublet lens onto a detector. MEMS inset image from Helmbrecht et al. (2011) [20].

perfect (due to the fact that during phasing not all segments are stowed), it proved more than adequate in removing the majority of the unwanted bias.

To determine the expected accuracy of the phasing method, several calibration datasets were taken and analysed, separately for piston and tip/tilt. The uncertainty caused by residual instability in the imaging system was estimated by analysing a sequence of images taken without moving any MEMS segments and computing their RMS scatter. This produced values of  $0.006 \mu\text{m}$  for piston and  $0.02$  milliradians (mrad) for tip/tilt, and was taken as an estimate of the uncertainty limit due to the stability of the setup.

One MEMS segment was then moved between two fixed positions several times to investigate the reproducibility of segment movements. This test showed that movement of the MEMS did not introduce any extra piston or tip/tilt to the moving segment beyond that expected due to stability with time. However, tilting one segment appeared to cause all other segments to move by a small amount. The RMS scatter of this motion was approximately  $0.10$  mrad, and appeared independent of the amount of applied tilt.

The movement resolution limits of the control software were  $0.02 \mu\text{m}$  in piston and  $0.02$  mrad for tip/tilt. Combining these sources of uncertainty sets an upper limit for the obtainable accuracy as  $0.02 \mu\text{m}$  in piston and  $0.10$  mrad in tip/tilt.

To test FICSM, random tilts and pistons were taken from a uniform distribution with limits of  $\pm 4 \mu\text{m}$  for piston and  $\pm 0.80$  mrad for tip/tilt. The piston values were chosen to be safely within the maximum possible range of motion of the MEMS segments, while the tilts were at a level where light from individual segments could easily be identified by eye but still provided some overlap. These values, along with the final results, are given in Table 1. The maximum possible piston between any two segments was then  $8 \mu\text{m}$ , approximately 1 coherence length.

Due to the fact that only relative pistons are measurable, a zero point must be chosen. In

order to ensure the pistons stayed within the range of motion of the MEMS, segment 2 was set to zero piston in the MEMS control software and the other segments measured relative to it. Tip/tilt, however, is defined relative to the centre of the image and so each image was centred on the same pixel to ensure a common phase centre.

During these tests, it was discovered that the measured pistons were as large as  $1.6\ \mu\text{m}$  when the segments were set to their nominal zero positions, and varied substantially from segment to segment. This is likely due to a combination of poor calibration of the preset MEMS “zero” position and wavefront errors from the various optical elements that formed the setup (collimator, mirrors and lens). This was expected, as the MEMS “zero” position is a manufacturer predefined configuration that is not a true reflection of a flat mirror. The final image is then a better indicator of image quality than the actual segment pistons and tip/tilts in the MEMS control software.

To ensure an identifiable target point for our phasing strategy, images with the segments set to zero were first analysed. The piston values measured in each filter were then subtracted from all future piston measurements. This ensured that the goal was to move the segments back to their manufacturer “zero” positions rather than to a new configuration (despite the fact that this may optimise the PSF). Indeed this is one of the strengths of FICSM; by directly measuring the wavefront it can be used to phase segments to an arbitrary, not-necessarily-cophased configuration.

These measured static pistons were later removed and a final image taken to demonstrate the accuracy of the measurements.

The sequence for phasing was modified slightly from the algorithm described earlier [12] since the negligible laser bandwidth used in the tip/tilt step made the need to repeat the entire procedure (as previously specified) unnecessary. Instead the tip/tilts were measured and removed once, while the pistons were measured and removed twice, with subsequent images

Table 1: Initial and final positions of each segment, measured at the wavefront.

Segment	Piston ( $\mu\text{m}$ )		Tip (mrad)		Tilt (mrad)	
	Initial	Final	Initial	Final	Initial	Final
2	1.70	0.00	0.78	-0.06	-0.76	-0.04
3	0.00	0.00	0.06	0.02	0.60	0.16
4	3.10	0.00	0.60	0.14	-0.30	0.18
5	-1.50	0.02	0.26	-0.14	0.34	-0.14
6	1.78	0.00	-0.14	0.04	-0.70	0.12
7	-0.64	-0.02	-0.16	-0.12	0.34	-0.14
8	3.20	0.04	-0.42	-0.08	-0.62	-0.08
9	-0.90	0.02	-0.28	0.00	-0.42	-0.02
10	1.78	0.00	0.40	-0.12	0.76	0.02
11	3.10	0.00	0.36	-0.10	0.80	0.20
12	-0.10	0.00	-0.44	0.14	-0.64	0.10
13	3.90	0.00	0.28	0.00	-0.44	0.06
14	1.26	0.00	-0.76	-0.08	0.70	0.08
15	-0.40	0.00	0.10	0.12	-0.40	-0.08
16	-3.18	-0.02	0.28	-0.14	0.74	-0.14
17	-0.04	0.00	0.40	0.06	-0.36	-0.02
18	1.42	0.00	-0.76	0.08	0.32	0.14
19	-3.14	0.00	-0.10	0.10	0.28	-0.24

taken to verify the setup. The modified sequence is as follows:

1. Take an image using the laser, measure tip/tilt.
2. Remove measured tip/tilt from the segments.
3. Repeat step 1 to verify the segment tip/tilts.
4. Take an image with each of the red and green broadband filters, measure piston.
5. Remove measured piston from the segments.
6. Repeat steps 4 and 5 once, followed by step 4 a third time to record the final segment positions.

## 6. Results

The initial and final positions of each segment are shown in Table 1. Any overall tip/tilt (due to the centring of the initial image) was removed. The pistons were reduced from a maximum of  $3.90\ \mu\text{m}$  to a maximum of  $0.04\ \mu\text{m}$ , while the tilts were reduced from a maximum of  $0.78\ \text{mrad}$  to a RMS scatter of  $0.12\ \text{mrad}$ .

Images taken using the configurations of each segment before and after phasing are shown in Fig. 3. The “after” image was taken with the mirror in its final configuration after phasing with the static wavefront error removed. For reference, a simulated image with a perfectly phased mirror and in the absence of noise is shown.

Upon examination of the phased images, it was apparent that the nominal segment “zero” positions produce a visually worse image than the FICSM phased solution. This is consistent with the observation of large measured static pistons for this “zero” setting.

The encircled energy as a function of radius from the peak was also computed to numerically compare the final image to the expected noise limit, and is shown in Fig. 4. Clearly, applying FICSM improves image quality substantially, and the encircled energy curve appears consistent with the noise limit. This corresponds to a RMS wavefront error of about  $25\ \text{nm}$ . This result suggests a Strehl ratio of 94% using the Maréchal approximation  $S = e^{-(2\pi\sigma/\lambda)^2}$ , where  $\lambda$  is the observing wavelength and  $\sigma$  is the RMS wavefront error.

This technique proved most sensitive to high Strehl ratio images, so an estimate of the initial Strehl ratio was given by multiplying the final Strehl ratio by the ratio of the peak fluxes of “before” and “after” images taken with the same exposure time. This yielded a value of 9%.

From these results it is clear FICSM has phased the mirror from a degraded state with large pistons beyond the longest filter coherence length and tilts at a level where individual segments could be identified by eye, to within the limits imposed by the segment control system.

## 7. Conclusion

Here we have experimentally demonstrated the Fizeau Interferometric Cophasing of Segmented Mirrors algorithm. 18 segments of a MEMS segmented mirror array were phased from a configuration with random initial piston steps of up to  $8\ \mu\text{m}$  and tilts of up to  $0.80\ \text{mrad}$ . The test was performed in the optical band (rather than the infrared) to maximise the aberrations produced by the limited-stroke mirrors. To phase the entire mirror, a segment-tilting approach was utilised. Suggested segment groupings were provided that allow an 18 segment mirror to be phased in 3 steps, assuming multiple simultaneous pointings on the detector are possible. Analysis of several sources of uncertainty produced an estimation of the final accuracy of  $0.10\ \text{mrad}$  in tip/tilt and  $0.02\ \mu\text{m}$  in piston. After a single application of FICSM to measure and remove tip/tilt and two applications to measure and remove piston, significant improvement in the PSF

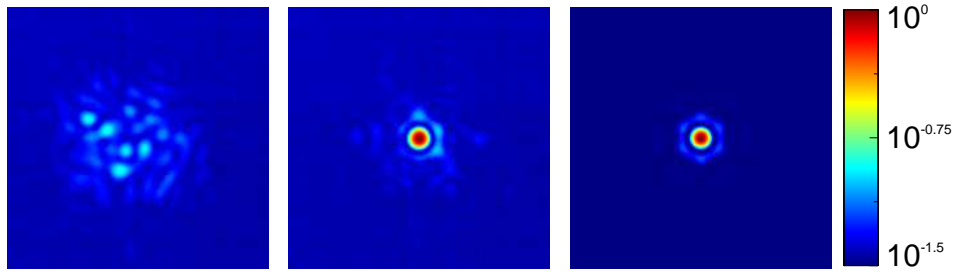


Fig. 3: Images showing the PSF before (left) and after (middle) phasing, with a log stretch. A simulated perfectly phased image (right) is also shown for comparison. Before phasing, power is spread over a large area. After applying FICSM, the PSF conforms well to the theoretical PSF in the absence of aberrations.

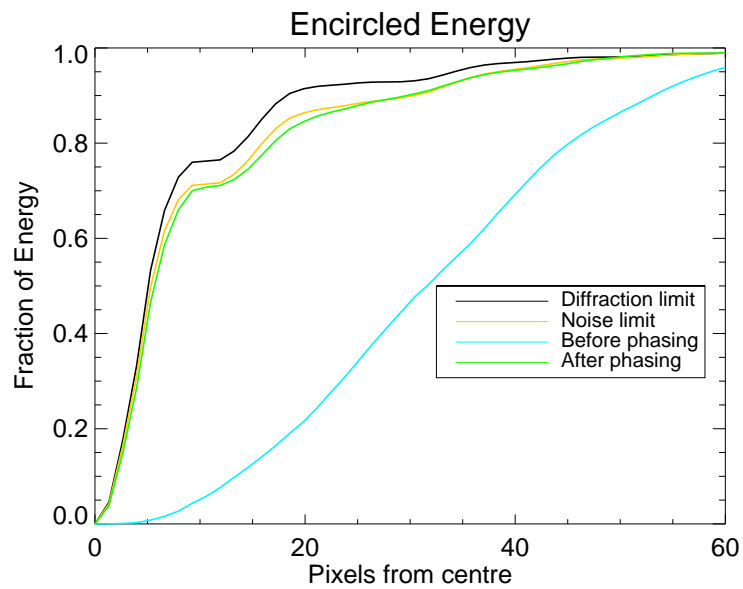


Fig. 4: The encircled energy as a function of radius of several real and numerical images. The black curve shows the result for a numerically generated image in the absence of noise and free of wavefront error. A typical example of a theoretically generated image with pistons and tilts consistent with the noise limit of the segments is shown in yellow. The blue and green curves show the results for real images taken before and after phasing. These results suggest that FICSM has successfully phased the mirror from an extremely degraded state to a level consistent with the expected noise.

of the setup was apparent. Comparing encircled energy diagrams for real and numerically generated images implied that the final setup is consistent with this limit, suggesting a final RMS wavefront error of 25 nm, or a Strehl ratio of 94%, from an initial Strehl ratio of 9%. This shows that FICSM has phased the mirror from its extremely degraded initial state to within the limit of accuracy imposed by the setup, using only a science camera, three filters and the actuated mirror itself.

### **Acknowledgments**

We acknowledge helpful discussions with Scott Acton and Edmund Nelan. We also wish to thank the anonymous reviewers for their helpful suggestions to improve the paper. Part of this research was supported by the Australian Research Council Centre of Excellence for Ultrahigh bandwidth Devices for Optical Systems (project number CE110001018). Part of this work was performed at the OptoFab node of the Australian National Fabrication Facility (ANFF). This work was also supported in part by the U.S. NASA grant APRA08-0117.